[1.]Boban KUSIGERSKI, [1.]Zoran PANDILOV, [2.]Goran KUSIGERSKI

# DESIGN AND PRACTICAL REALIZATION OF A SCARA ROBOT

[1.]Institute of Production Engineering and Management, Faculty of Mechanical Engineering, SS. Cyril and Methodius University in Skopje, N. MACEDONIA
[2.]Replek Farm LTD, Municipality of Skopje, Kozle 188, Skopje, N. MACEDONIA

**Abstract:** This research presents the design and prototyping of a SCARA robotic arm with 3 degrees of freedom. This student project is sponsored by the Faculty of Mechanical Engineering, Skopje, Republic of N. Macedonia. Therefore, there are certain prerequisites that need to be fulfilled, in terms of cost and functionality, without sacrificing structural rigidity and functionality. For this reason, standardised elements and 3D printed components are used for the structure and transmission. The motion of the robotic arm is achieved by using inverse kinematics and path control. Multiple graphic models of velocity profiles (trapezoidal and S – curve) are compared for calibrating the motion smoothness. The end effector uses a pneumatic vacuum system for gripping and transferring objects with weight less than 250 g. Drive and control elements such as stepper and DC motors, sensors and encoders allow for the implementation of a feedback loop for more precise functioning of the SCARA robotic arm. Multiple control modes are further detailed. The study at the end gives a review of the obtained precision and achieved motion capabilities, considering the cost-efficiency and proposing steps for further improvement of realisation and replication on a larger scale.

**Keywords:** SCARA robotic arm, inverse kinematics, velocity profiles, acceleration, jerk, 3D printing

## INTRODUCTION

Throughout history, the standard methods of manufacturing were subject to intensive changes. The use of industrial robots begins in the 1960's with CAD (Computer Aided Design) and CAM (Computer Aided Manufacturing) systems, which continuously expanding. The advantages [1] for introducing industrial robots in manufacturing are:

- increased productivity;
- reduced labour costs [2];
- eliminating routine tasks with repetitive work cycles [3];
- increased worker safety;
- completion of processes that can't be done manually or are done in a dangerous environment [4];
- reduced use of raw material;
- increased flexibility [5];
- improved manufacturing quality and tolerances [6];
- improved repeatability.

The use of robots in various industries is becoming more and more prevalent, and the number of robots implemented in manufacturing, military, food preparation, etc., continuously rising [7]. The goal of this research paper is the analysis of the issues that arise in the design and prototyping of a SCARA robotic arm. The type of SCARA robotic arm developed in this research work contains 3 degrees of freedom, due to the simplicity for its realization. Nevertheless, the basic components and principles applied are the same as in a higher complexity industrial robot.

SCARA is an acronym for Selective Compliance Assembly Robot Arm. The acronym refers to the design of robot arm which enables relatively ease positioning in the x, y plane, while it is still enough rigid in the z-axis. This characteristic has proven itself fairly sufficient in assembly and loading/unloading processes.

Most industrial robots use mechanical components and materials with high costs and their electronics is commercially designed. Due to the fact that this project is sponsored by the Faculty of Mechanical Engineering, Skopje, Republic of N. Macedonia, there were certain prerequisites that need to be fulfilled:

- The use of standard mechanical elements and 3D printed elements;
- The use of standard electronic components and a low-cost microcontroller.

The prototype is for a robotic arm with 3 degrees of freedom, more precisely 2 rotations of the links (shoulder and elbow) and one translation in the vertical direction (Figure 1). The shoulder and elbow allow precise positioning in the x,y plane, and the translation is used for exact positioning in vertical z – axis, i.e., pick and place the objects.

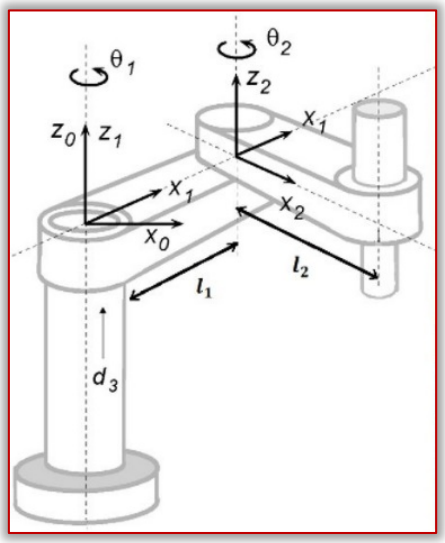


Figure 1: Coordinate systems and concept of the robotic arm [8]

## KINEMATICS AND MOTION CONTROL

The positioning of robots is done by using direct kinematics, where the length of the links and the rotational angle of each of the joints of the robotic arm is used in order to

calculate the position of the end effector in a Cartesian coordinate system.

Inverse kinematics is used during the positioning of robotic end effectors in order to calculate the angular rotation of each of the joints for a known length of the links. This allows to calculate the rotational angles S, Q and E (Eq. 1, 2 and 3), for known x and y coordinates, which represent the coordinates where the end effector should be positioned at the end of the movement (Table 2).

Table 1: Precision (resolution) calculations by using different parameters

| Link length (mm) | Number of microsteps for 1 rotation of the motor | Pulley reduction | Arc resolution (mm/step) | Torque (Nm) |
|---|---|---|---|---|
| 300 | 1600 | 1:5 | 0,24 | Shoulder motor 11,5 |
| 600 | 1600 | 1:5 | 0,47 | Elbow motor 4,5 |
| 300 | 800 | 1:20 | 0,12 | Shoulder motor 46 |
| 600 | 800 | 1:20 | 0,24 | Elbow motor 18 |
| 300 | 200 | 1:20 | 0,47 | Shoulder motor 46 |
| 600 | 200 | 1:20 | 0,94 | Elbow motor 18 |

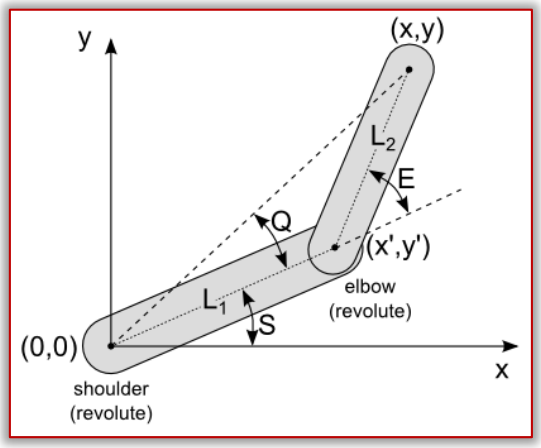


Figure 2: Trigonometry angles of SCARA inverse kinematics [9]

In order to calculate each of the angles, the following trigonometric formulas [9] are used:

$$E = \arccos\left(\frac{x^2+y^2-L_1{}^2-L_2{}^2}{2L_1L_2}\right) \quad (1)$$

$$Q = \arctan\left(\frac{L_2 \sin E}{L_1+L_2*\cos E}\right) \quad (2)$$

$$S = \arctan\left(\frac{y}{x}\right) - Q \quad (3)$$

where: x, y – the known coordinates of the end effector at the end of its path;

$L_1$ and $L_2$ – length of each of the links (shoulder and elbow).

Table 2: Inverse kinematics calculations for given x and y coordinates

| x | y | $L_1$ (mm) | $L_2$ (mm) | Q | Q (°) | S | S (°) | E | E (°) |
|---|---|---|---|---|---|---|---|---|---|
| 10 | 50 | 32,7 | 32,7 | 0,67666312 | 39,0 | 0,6929506 | 39,7 | 1,3609 | 78,0 |
| 10 | -50 | 32,7 | 32,7 | 0,67666312 | 39,0 | -2,053851 | -117,7 | 1,3609 | 78,0 |
| 50 | 30 | 32,7 | 32,7 | 0,46996783 | 27,3 | 0,0644843 | 3,7 | 0,95187 | 54,5 |
| 65,4 | 0 | 32,7 | 32,7 | $1,75\cdot10^{-6}$ | 0,0 | $-1,75\cdot10^{-6}$ | 0,0 | $3,49\cdot10^{-6}$ | 0,0 |

To achieve higher precision, the actuation of the links is done by using stepper motors (satisfying the above-mentioned prerequisites) with 200 steps per revolution with stepper drivers that allow each step to be additionally divided into smaller microsteps. Additionally, the belt and pulleys used to transmit motor revolutions to the link shafts allow an increase in the precision and torque (M=2.3 Nm on the shoulder and M=0.9 Nm for the elbow) (Table 1).

The use of 1:8 microstepping ratio (1600 microsteps) and pulley transmission ratio of 1:5 allows for a high precision and torque compared to other combinations of microstepping and transmission, without compromising the positional speed of the robotic arm to a great extent. The robotic arm is set to work in the first and forth quadrant for the angles E and Q (Figure 2) in order always to have a positive value, while the value of the angle S dictates in which quadrant the end effector will be positioned. The movement of the robotic arm is done by using a point-to-point path. For this kind of control, the current (start) and end point of the end effector are inputs and the processor generates the path between them, meaning that during the movement between start and endpoint, no useful operations can be performed.

Hence, the trajectory between start and end point, is not as important as the position at the end of the movement. In order robotic arm to position itself, as fast as possible, all the joints move at the same time. The time necessary for the joint with the biggest angular rotation to position itself, is taken as the reference time needed for positioning [10]. If it is required for the robotic arm to complete multiple movements in one sequence, then the inverse kinematics is calculated from the start point to the first point of movement. After the first point of movement is reached then the current coordinates are replaced as the start point and the inverse kinematics is calculated for the second point of movement. This calculation repeats itself in accordance to how many points the end effector has to move to.

## SPEED, ACCELERATION AND JERK

The efficiency of robots [11] is measured by their speed and positional precision. The errors that happen during operation, most often are due to overloading or high accelerations, which causes the motors to lose their positional accuracy because of the system inertia. Jerk is defined as the change of acceleration with respect to time. It is the first derivative of acceleration (the third derivative of position).

$$\text{Speed: } \lim_{t\to 0}\frac{dx}{dt} = x'(t) = V\left(\frac{m}{s}\right)$$

$$\text{Acceleration: } \lim_{t\to 0}\frac{dV}{dt} = x''(t) = a\ \left(\frac{m}{s^2}\right)$$

$$\text{Jerk: } \lim_{t\to 0}\frac{da}{dt} = x'''(t) = j\left(\frac{m}{s^3}\right)$$

The relationship between position and the first, second and third derivative of position with respect to time is graphically presented in Figure 3. In the time frame $t_0$-$t_1$, the travel distance linearly increases, which means that the speed increases following a certain function. The increase and decrease of speed indicate a change in acceleration in the time frames $t_0$-$t_1$ and $t_2$-$t_3$ while during $t_1$-$t_2$ the change in acceleration is not existing. During the time frames when

there is a change in the acceleration, the jerk has the highest value. If there is no change in acceleration then the jerk has a value of 0.

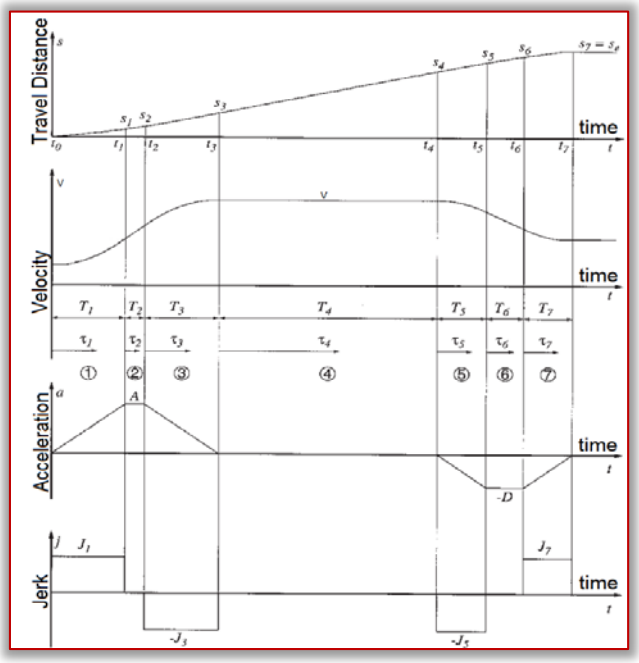


Figure 3: The relationship between position, speed, acceleration and jerk [12]

The problems that jerk causes in physical systems [13] affect motion and stability, more specifically it excites oscillations that increase the settling time and decrease position accuracy. This increases the need for the jerk to be lowered as much as possible without hindering the functionality at great extent (making the robot to have very slow accelerations/decelerations), which is accomplished by using trajectory profiles. A trapezoidal trajectory profile (Figure 4), has a sudden acceleration to a certain value, keeps the value for a certain period, then suddenly decelerates to 0. This generates a trapezoidal curve for the velocity with respect to time. The corners (α=90°) of the rectangle that point to the changes in acceleration correspond with time when the jerk theoretically has an infinite value, because of the sudden change of acceleration from 0 to maximum value or from maximum value to 0. This kind of profile is used in milling, dispensing and painting applications where the change in speed needs to be linear.

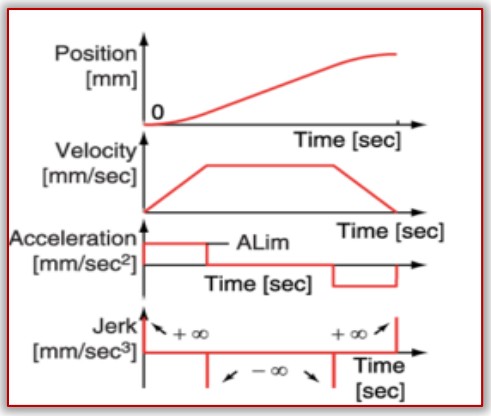


Figure 4: Trapezoidal velocity profile and its effect on acceleration and jerk [14]

To reduce the high jerk values, the move profile is done by using an S-curve velocity profile (Figure 5). The acceleration in S-curve velocity has a trapezoidal profile (α<90°), meaning that the change in acceleration is linear, which enables reducing the jerk.

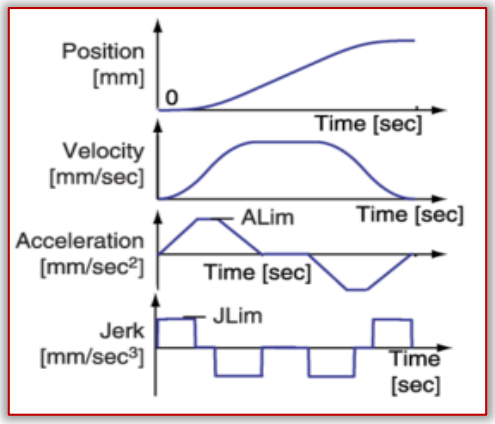


Figure 5: S–curve velocity profile and its effect on acceleration and jerk [14]

In this case study, multiple velocity S-curves have been calculated and compared in order to choose the most suitable one which satisfies the needs of the robotic arm. The trapezoidal profiles represent the change in acceleration from initial (0 mm/s$^2$) to maximal, with increments of 0.01 mm/s$^2$ multiplied by their corresponding acceleration coefficient. The four velocity S-curves have different acceleration coefficients: $a_4$=0.75, $a_3$=0.8, $a_2$=0.9 and $a_1$=1 (Figure 6) and different frequencies at which the increments are sent to the motor: $a_4$=250 Hz, $a_3$=240 Hz, $a_2$=220 Hz and $a_1$=200 Hz, meaning that in the same period, a different number of increments can be sent i.e., different maximum accelerations and speeds can be reached. The $a_1$ curve has the biggest increments in acceleration, but the number of increments sent to the motor is the lowest, while opposite, the $a_4$ curve has the smallest acceleration increments, but the highest number of increments. The $a_1$ curve increases the acceleration in the first 50 impulses with 0.01 mm/s$^2$ increments, in the next 100 impulses the acceleration has a fixed value and in the last 50 impulses the acceleration is reduced by 0.01 mm/s$^2$ increments until the maximum speed is reached. The $a_4$ curve increases the acceleration in the first 75 impulses with 0.0075 mm/s$^2$ increments, in the next 100 impulses the acceleration is stable, and in the last 75 impulses the acceleration is reduced by the same incremental value which was used for acceleration. Then the movement continues with the maximum speed, until reaching about 200 impulses of the end position for the $a_1$ curve (or 250 for the $a_4$ curve), when the inverse process of the above-explained starts, following a symmetrical curve. The profile ends when the starting speed is reached.

Comparing the four trapezoidal acceleration curves, we can observe the change in acceleration is highest in the $a_1$ curve and lowest in the $a_4$ curve. Thus, the goal of reducing the jerk is achieved. Also, due to the bigger number of increments, the maximum speed ($V_4$=98.4 mm/s) that the $a_4$ curve can reach, is bigger than the maximum speed ($V_1$=75

mm/s) that the $a_1$ curve can achieve. Both the reduced jerk and the higher maximum speed (Figure 7) allow the reduced oscillations and wear of the mechanical elements. For the above-mentioned reasons the $a_4$ curve is selected as the move profile for the robotic arm.

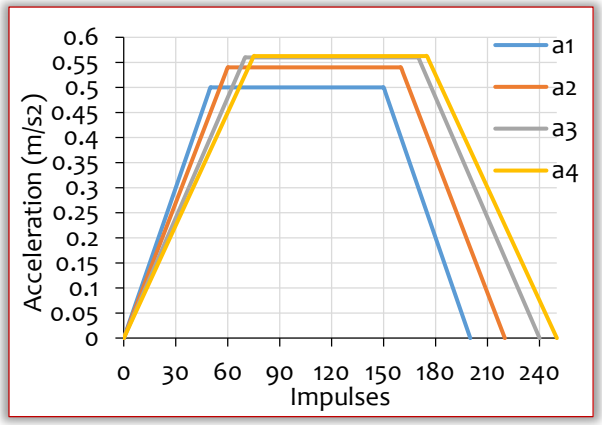


Figure 6: Comparison of trapezoidal acceleration curves

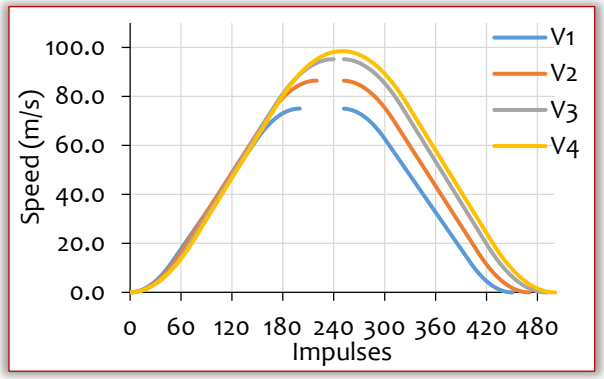


Figure 7: Comparison of different S velocity profiles

## MECHANICAL ELEMENTS

The mechanical components used in the robotic arm assembly (Figure 8) can be divided by their purpose in three categories:

- Structural components, which comprise the robotic arm and allow better rigidity;
- Transmission elements, which transmit motor drives torque to the shafts;
- Fasting and standard elements, such as bolts, nuts, bearings, etc.

The structural elements are: extruded aluminium profiles, platform, 3D printed components and linear rails. Aluminium is chosen for its easy machining, availability and lesser density than steel (2.7 gm/cm$^3$ versus 8g/cm$^3$).

The assembly uses 4 profiles (2 for the shoulder and 2 for the elbow) with dimensions 20x20x300 mm made from aluminium 6063-T5. The profiles are vertically interlocked by specially designed 3D printed components that increase the rigidity of the assembly.

The aluminium platform, which travels in the z-axis direction is used as the base for the robotic arm. The linear rails on which the whole platform travels are type SBR-12 (l=400mm) and the linear bearings that travel on them are fastened with bolts to the aluminium platform. This allows movement of the whole robotic assembly of 300 mm in the z-axis.

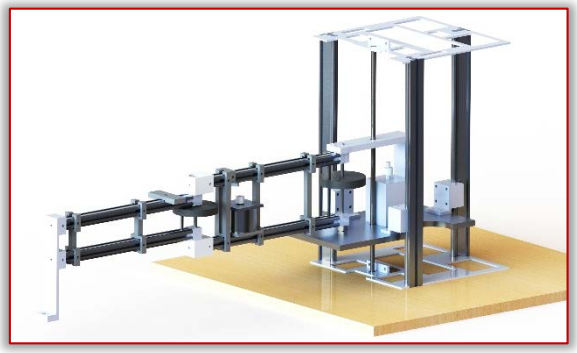

Figure 8: CAD of the robotic arm assembly modelled in Solidworks

The 3D printed components are made by using a FDM (Fused Deposition Modeling) 3D printer using PLA (Polylactic Acid) plastic, which is the cheapest, most available and easiest to use for prototyping purposes, while also having fairly satisfactory mechanical properties [15].

The structural 3D printed components (Figure 9) in the assembly are: frames that interlock the aluminium profiles together (1), housings for the ball bearings that connect to the elbow shaft (2), limit switch support (3), motor, encoder and vacuum suction cup bases (4), frame for precise positioning of the linear rails (5), etc. These components were designed in Solidworks [16] and sliced in Cura, using 0,2 mm layer height and 15-40% infill, for a combination of fast prototyping and low mass.

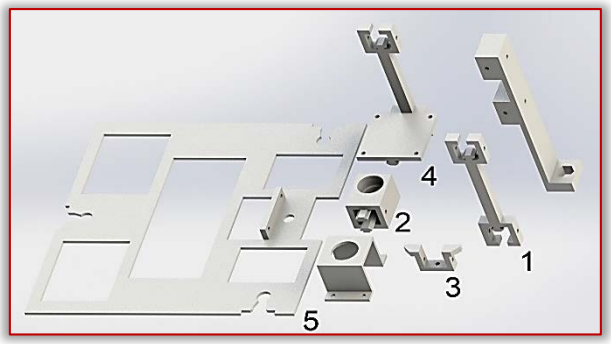


Figure 8: Solidworks CAD models of 3D printed components

The use transmission elements are: threaded rod, belts and pulleys and elastic shaft couplings.

The threaded rod used for the z-axis movement is with an 8mm pitch and is connected to the platform via a threaded nut. The threaded rod is driven by a DC motor using an HTD (High Torque Drive) profile belt, and a pulley reduction ratio of 1:5. This allows speed reduction, higher torque and increased precision. If a lower transmission ratio is used, the motor would not have enough torque to move the aluminium platform and the robotic arm attached to it, while a bigger transmission ratio would reduce the speed of the z-axis movement to a greater extent. The pulleys are 3D printed and parametrically designed by using Solid 3D CAD modeller OpenSCAD. The other 2 pairs of pulleys for the shoulder HTD (High Torque Drive) and elbow (XL – extra light) drive are designed using the same method. The

encoders on the z-axis and the elbow are connected to the shafts by elastic couplings which allow compensation for axial misalignment.

Figure 10: DC motor connected to a threaded rod via belt and pulley mechanism

## DRIVE ELEMENTS

The electric drive elements in the robotic arm are stepper motors and DC motor.

The stepper motors used in the robotic arm have 200 steps (1.8°/step), and the drivers are configured for 8 microsteps for each step. This increases the resolution of the movement to 0.225°/step. The stepper motor used for driving the shoulder (Figure 11) has a torque of M=2.3 Nm and the motor for the elbow (Figure 12) has a torque of M=0.9 Nm. Because the elbow motor is mounted on the shoulder member, there are weight restrictions. It has to be with low mass, which results in low torque. The possibility of missed steps due to jerk, low torque, high speed or weight is compensated by installing an encoder with a positional feedback loop.

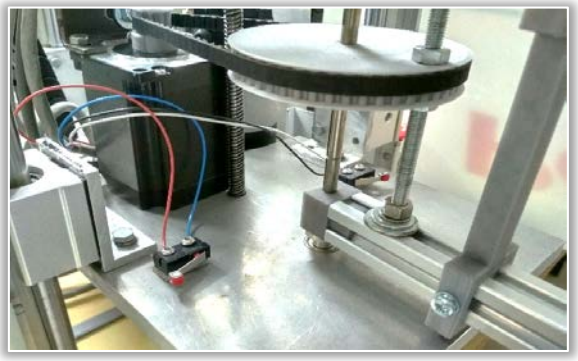

Figure 11: Pulley and motor assembly for shoulder

Figure 12: Pulley and motor assembly for elbow

The DC motor used in the robotic arm is used for moving the platform and the end effector in the z-axis. It has a torque of M=0.94 Nm and is driven by PWM (Pulse Width Modulation) using an H-bridge, which switches the polarity of the motor and allows rotation in both directions. The DC motor, just like the elbow drive motor is coupled with an encoder for positional feedback loop, to allow for precise real-time positioning of the robotic arm.

## PNEUMATICS

The end effector of the robotic arm uses a pneumatic system comprised of several parts: pneumatic compressor, pneumatic tubes, pneumatic solenoid valve 5/2, vacuum generator and vacuum suction cup [17]. The compressor creates vacuum that can either stay trapped (closed valve position) or go to the vacuum generator (open valve position). The vacuum generator creates a vacuum (P= - 0.9 bar) and it is connected to the vacuum suction cup which has an outer diameter of d=14 mm and can lift objects with mass less than m < 250g. The activation of the valve is done by the microcontroller.

## SENSORS

Several sensors are applied in the robotic arm, like incremental positional encoders, limit switches and optical limit sensors.

Due to the fact that the position of the incremental positional encoders mounted on the elbow and z-axis is unknown after each start of the robotic arm, each of the links have to return to their reference position (going to zero point procedure) in order encoder to obtain data from where to start the counting the rotational angle. The encoders have a resolution of 2000 impulses/rotation i.e., a resolution of $\frac{360^\circ}{2000} = 0.18^\circ$. The mechanical limit switches on the robotic arm are placed on the start and end position of the rotational angle (2 limit switches for the shoulder and 2 limit switches for the elbow) (Figure 11 and 12). They are used as a security devices which will not allow motors to do a larger movement than the assembly physically allows, preventing collisions and deformations. The other use for the limit switches is mentioned above for the finding the "zero point" of the links.

The optical limit sensors used in the robotic arm find application in limiting the minimum and maximum move of the z-axis platform. They are positioned in the lowest and highest move points of the platform, not allowing colliding with the other elements. When the L-profile attached to the platform, interrupts the laser beam of the sensor, the DC motor gets a command to stop the rotation and the movement of the platform. This is also used for the above-mentioned procedure of finding the "zero point" the platform.

## CONTROL ELEMENTS

The main control element in the robotic arm is the Arduino Mega microcontroller. For supplying voltage to the stepper motors and the pneumatic valve a 230 V AC to 24 V DC power supply is used, with a limiting current of maximum 10A. For supplying voltage to the z-axis DC motor, the voltage is additionally lowered to 18 V DC. The Arduino

microcontroller and the limit switches have a working voltage of 12 V DC, and the encoders are directly connected to the microcontroller using its 5 V DC output pins.

The control of the robotic arm is done on two levels.

On the first level, the robotic arm is controlled by the microcontroller performing the following tasks:

- Reading inputs from the mechanical limit switches and optical limit sensors and reading the positional feedback from the encoders;
- Driving the stepper and DC motors;
- Controlling the pneumatic solenoid valve;
- Communicating with the second (higher) level of control via USB.

The second control level is done on a PC, by using a SCADA (Supervisory Control And Data Acquisition) application with the following tasks:

- Communicating with the microcontroller;
- User interface for manual input of coordinates for the end effector (Figure 13);
- Automatic movement of the robotic arm to coordinates input from computer vision or text files;
- Sequence activation (teach mode) in which the robotic arm positions itself in manually defined positions and afterward calculates its path;
- Inverse kinematics calculations i.e., the number of impulses needed for rotating each of the links to the end coordinates of the end effector.

On the user interface (Figure13) the $X_1$ and $Y_1$ are the starting coordinates of the end effector and $X_2$ and $Y_2$ are the coordinates which have to be input as the end-of-path coordinates. $L_1$ and $L_2$ are the link lengths, the microstep field is for the multiplication factor of microstepping characteristic of the stepper drivers, and the offset field is for defining an offset, so that the number of steps the motors have to realize is not negative. These values have to be an input for the inverse kinematics calculations. With the "calculate" button, the inverse kinematics are calculated and all of the angles E, Q, S, $E_2$, $Q_2$, $S_2$ are shown in degrees.

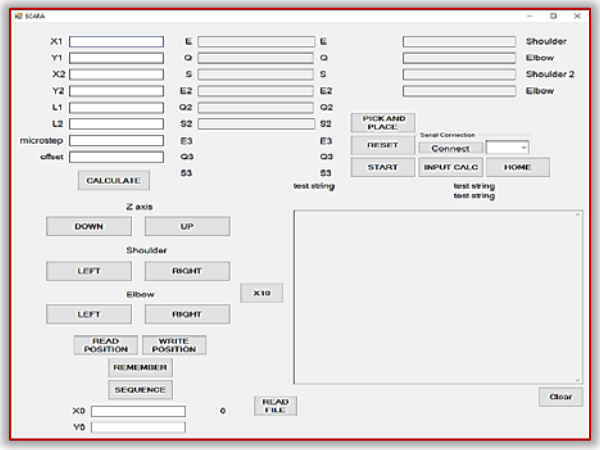


Figure 13: SCADA application for control of the robotic arm

For manual control there are separate jog buttons with variable speed (X1 or X10) for the shoulder, elbow and platform. For automatic control of the robotic arm and doing pick and place operations, there are 2 different operation modes, with previously entered coordinates or with teach mode.

By pressing "read file", the text file (which is automatically generated by using computer vision or by manually inputting coordinates of objects that need to be moved) is loaded into the application. Then by pressing the "pick and place" button the robotic arm first position itself by hitting all 3 home limit switches (minimum rotation elbow and shoulder and minimum z-axis position) and afterwards it goes to the first point, picks the object up, and takes it to a previously defined end coordinate ($X_0$,$Y_0$) where all of the objects need to be placed. Then the robotic arm continues from the $X_0$,$Y_0$ position to the second object, and repeats the process for all objects.

The other operation mode is sequential control in teach mode. The robotic arm, in fact the end effector is positioned above the object that needs to be moved (point 1), the "remember" button is pressed and afterwards the robotic arm is manually jogged to the end position where the object needs to be positioned (point 2) and the "remember" button is pressed again. With the press of the "sequence" button the robotic arm "finds zero position" and goes to the point 1, picks the object up, moves to point 2 and puts the object down. Afterwards the end effector goes to point 1 and repeats the process according the instructions of the operator of the robotic arm.

## CONCLUSIONS

The final assembly of the SCARA robotic arm (Figure 14) satisfy all the criteria mentioned at the beginning of this paper: the use of low cost and standard components and the use of 3D printed parts.

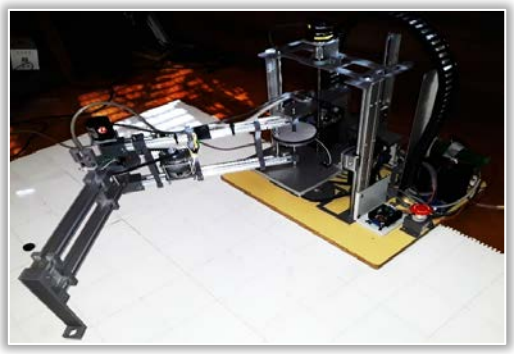

Figure 14: Final look of the SCARA robotic arm

The results that are achieved are similar and within tolerance of the results obtained through the calculations. The maximum z-axis movement of the robotic arm is 300 mm, the maximum rotational angles of the shoulder and elbow are 180° and more than 185°, respectively. The repeatability is less than 2 mm in teach mode, and less than 4 mm in sequence mode due to the mechanical limitations of the robotic arm. These values are convenient for uses such as spraying or painting, spot-welding, assembly or transport to a conveyor belt. For industrial needs the SCARA robotic arm can be replicated with bigger dimensions and work area as well as a larger load carrying capacity.

Additionally, the robotic arm can be further improved by:

- Increasing the rigidity of the mechanical assembly for better precision;
- Decreasing the position time by replacing the stepper motors with servo motors;
- Introducing a system of laser measurement of the objects height for more precise z-axis positioning;
- Fully integrating a computer vision system, which along with the laser measuring system will make the robotic arm almost fully autonomous;
- Finding a commercial use of the robotic arm.

## References

[1] R. Miller and M. R. Miller, Robots and Robotics : Principles, Systems, and Industrial Applications. 2017.
[2] J. H. Jung and D. G. Lim, "Industrial robots, employment growth, and labor cost: A simultaneous equation analysis," Technol Forecast Soc Change, Vol. 159, Oct. 2020
[3] A. A. Wasique, D. Paritosh, P. Sahishnu, and P. Sunita, "A Review on Robotic Process Automation," International Conference on Advances in Science & Technology, 2019
[4] J. Petereit, J. Beyerer, T. Asfour, S. Gentes, and B. Hein, ROBDEKON: Robotic Systems for Decontamination in Hazardous Environments. Würzburg: 2019 IEEE International Symposium on Safety, Security, and Rescue Robotics (SSRR), 2019.
[5] A. C. Bavelos et al., "Enabling flexibility in manufacturing by integrating shopfloor and process perception for mobile robot workers," Applied Sciences (Switzerland), Vol. 11, No. 9, 2021
[6] A. Verl, A. Valente, S. Melkote, C. Brecher, E. Ozturk, and L. T. Tunc, "Robots in machining," CIRP Annals, Vol. 68, No. 2, pp. 799–822, Jan. 2019
[7] M. Guerry and C. Müller, "World Robotics 2021," 2021.
[8] M. E. Uk, F. B. Sajjad Ali Shah, M. Soyaslan, and O. Eldogan, "Modeling, control, and simulation of a SCARA PRR-type robot manipulator," Scientia Iranica, Vol. 27, No. 1, pp. 330–340, Jan. 2020
[9] N. Surapong and C. Mitsantisuk, "Position and Force Control of the SCARA Robot Based on Disturbance Observer," in Procedia Computer Science, 2016, Vol. 86, pp. 116–119
[10] K. (Kevin M. ) Lynch and F. C. Park, Modern robotics : mechanics, planning, and control. 2017.
[11] F. Stuhlenmiller, S. Weyand, J. Jungblut, L. Schebek, D. Clever, and S. Rinderknecht, "Impact of cycle time and payload of an industrial robot on resource efficiency," Robotics, Vol. 10, No. 1, pp. 1–18, Mar. 2021
[12] K. Erkorkmaz and Y. Altintas, "High speed CNC system design. Part I: Jerk limited trajectory generation and quintic spline interpolation," Int J Mach Tools Manuf, Vol. 41, No. 9, pp. 1323–1345, Jul. 2001
[13] J. J. Craig, P. Prentice, and P. P. Hall, "Introduction to Robotics: Mechanics and Control Fourth Edition," 2022.
[14] C. H. Yeung, Y. Altintas, and K. Erkorkmaz, "Virtual CNC system. Part I. System architecture," Int J Mach Tools Manuf, Vol. 46, No. 10, pp. 1107–1123, Aug. 2006
[15] S. A. Raj, E. Muthukumaran, and K. Jayakrishna, "A Case Study of 3D Printed PLA and Its Mechanical Properties," 2018.
[16] David C. Planchard, Engineering Design with SOLIDWORKS 2020. 2020.
[17] E. Papadakis, F. Raptopoulos, M. Koskinopoulou, and M. Maniadakis, "On the Use of Vacuum Technology for Applied Robotic Systems," International Conference on Mechatronics and Robotics Engineering, Vol. 6, pp. 73–77, 2020.

ISSN: 2067–3809